$^{59}Co(^{16}O,^{16}O)^{59}Co$ elastic scattering

N. B. J. Tannous, J. F. Mateja, D. C. Wilson,* L. R. Medsker, and R. H. Davis
Department of Physics, Florida State University, Tallahassee, Florida 32306
(Received 14 February 1978)

Differential cross sections for the $^{59}Co(^{16}O, ^{16}O)^{59}Co$ elastic scattering have been measured at laboratory energies 36, 40, 45.5, 49, 52, and 56 MeV. The angular range was 15°–170° (lab) in 5° steps at lower energies. At higher energies detailed angular distributions were carried out in 1° steps until the ratio to Rutherford was $< 10^{-3}$ with sample measurements at larger angles to assure that the differential cross sections were less than 10^{-4} ratio to Rutherford. The data have been analyzed with a four parameter optical model and the continuous ambiguities in this model are discussed. Strong absorption radii and the values of the nuclear potentials at these points are determined. Good fits to the data have been obtained using a G-matrix double-folding model with double-folded or Woods-Saxon forms for the imaginary potential. The required normalization of the real double-folded potential is near unity for all energies. Total reaction cross sections have been obtained by the optical model, quarter-point, "half partial-wave," and the sum of differences methods. The sum of differences method gives slightly larger total reaction cross sections than do the other methods by an amount consistent with estimates of the Coulomb excitation cross section. Estimates of the errors in the sum of differences values are computed by applying the optical theorem and are shown to be negligibly small.

[NUCLEAR REACTIONS: $^{59}Co(^{16}O,^{16}O)\,^{59}Co$; measured $\sigma(\theta,E)$, E_{lab}= 36, 40, 45.5, 49, 52, and 56 MeV; measured total reaction cross sections.]

I. INTRODUCTION

The elastic scattering of ^{16}O has been studied for ^{56}Fe, $^{70,74}Ge$, and ^{90}Zr,[1] the even Ni isotopes,[2] and the odd Cu isotopes[3,4] at various energies from the barrier up to approximately 60 MeV (lab). The present study of the elastic scattering of ^{16}O by ^{59}Co at $E_{lab}=36$–56 MeV extends the systematics for ^{16}O scattering by targets near $A \sim 60$. Detailed angular distributions were measured to assure precise determinations of the total reaction cross sections by the sum-of-differences (SOD) method.[3,5] Total reaction cross sections are obtained by the SOD, optical model, quarter-point,[6] and "half partial-wave" methods. Recent, but seemingly disparate experiments on Coulomb excitation and total fusion reaction studies have revived an interest in total reaction cross section measurements.[7]

The data have been analyzed using a standard four parameter Woods-Saxon optical model. The continuous ambiguities in this model are discussed and the parameters obtained are compared with the results for neighboring nuclides.[2-4] Fits to the experimental differential cross sections have also been obtained using a G-matrix double-folding model developed at the Oak Ridge National Laboratory[8] and Florida State University.[4,9] This model has been incorporated in the computer code JIB[10] by Stanley and Golin. This "one and one-half" parameter model has previously been used with success[4,8,9] in describing the experimental data of Refs. 1, 2, and 4.

An estimate of the error in the SOD determination of the total reaction cross section is made by applying the optical theorem.[11] It is vanishingly small at low energies and only a few percent at the highest bombarding energies.

Experimental procedures are discussed and data presented in Sec. II. The results of scattering potential analyses, both optical model and double-folded models, are given in Sec. III. Comparisons with results for other targets in the $A \sim 60$ region are also made here. Section IV contains the results of total reaction cross section determinations.

II. EXPERIMENTAL PROCEDURE

The Florida State University Super FN tandem Van de Graaff accelerator was used to produce a 36- to 56-MeV ^{16}O beam of charge state +5 or +6 from an inverted sputter source.[12] The beam impinged upon 30 to 50 $\mu g/cm^2$ of ^{59}Co target material deposited on 15 to 25 $\mu g/cm^2$ of ^{12}C backing foil. In this experiment, an array of six Si surface barrier detectors of 100 μm depletion depth were mounted 10° apart in a wedge fixed to a rotatable table in a 45 cm diameter scattering chamber.[13] Up to 66-point elastic scattering angular distributions ($\Delta\theta=1°$ lab) were measured. A seventh Si surface barrier detector of the same depletion depth was used as monitor. The Rutherford scattering of ^{16}O nuclei by 75 to 100 $\mu g/cm^2$ self-supporting ^{197}Au targets was used for energy calibra-

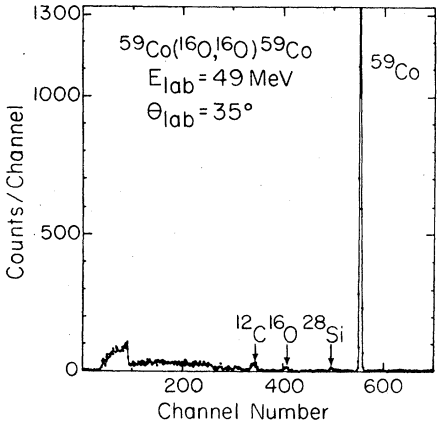

FIG. 1. Measured pulse height distribution for ^{16}O on ^{59}Co at E_{lab} = 49 MeV, θ_{lab} = 35°.

tion and normalization.

A typical pulse height distribution is displayed in Fig. 1. Energy resolution ranged from 350 to 500 keV. This is energetically sufficient to separate the yield of inelastically scattered particles, but as illustrated by Fig. 1, the inelastic yield was too small for detection in this experiment.

After conversion in fast analog-to-digital converter (ADC) units, data were processed and stored in the Univac (EMR) 6130 computer. Analyses of the data were performed on the Harris (Datacraft) 6024/3 computer located in the tandem accelerator laboratory.

III. DATA AND POTENTIAL MODEL ANALYSES

A. Optical model analyses

The measured angular distributions for the elastic scattering of ^{16}O by ^{59}Co are presented in Fig. 2. The data have been submitted for deposit in PAPS.[14] Sample error bars are shown in Fig. 2 for the back-angle points and for several points which fall outside the otherwise smooth locus of the data points. The errors are typically about ±3% at forward angles, as much as twice that value near the break from Rutherford, and monotonically increase to the back-angle values shown in Fig. 2. Because of the large number of points, the conservative error estimates, and the accuracy with which the several models reproduce the experimental angular distributions, rather small values of normalized χ^2 (defined below) are obtained as shown in Tables I and II. The computed curves were calculated with the nuclear optical model and two versions of a G-matrix double-folded potential model.[4,8,9] Analysis with the double-folding models is discussed in the next subsection.

The first objective of the present optical model analysis, after confirming the absence of discrete

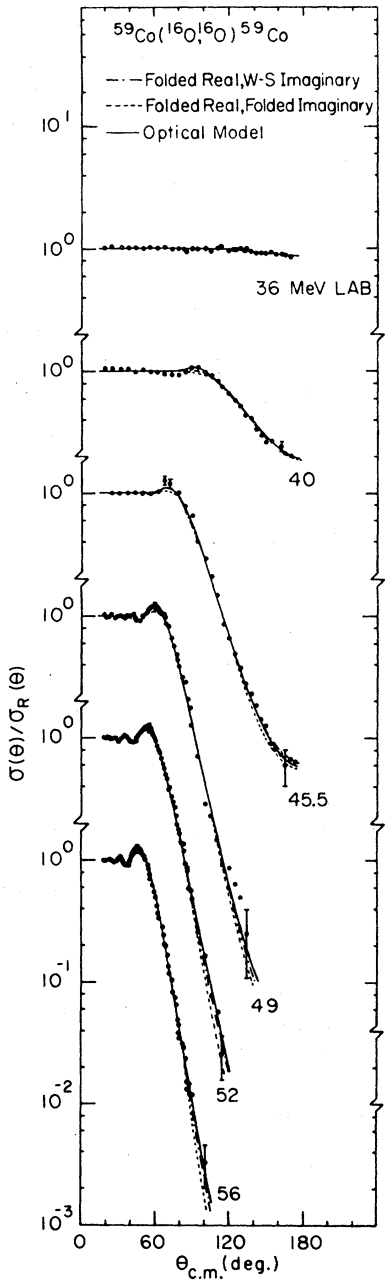

FIG. 2. Experimental angular distributions for ^{59}Co(^{16}O,^{16}O)^{59}Co at E_{lab} = 36–56 MeV. The curves show optical, double-folding real and imaginary, and double-folding real with Woods-Saxon imaginary model fits.

ambiguities, is the determination of the constants for the continuous ambiguities. Two values of the potential are fixed by a measured angular distribution, the real nuclear potential at the strong absorption radius and, somewhat less precisely, the barrier height.[1,2,4,8,9] The second objective is a demonstration of the stability of these two quanti-

TABLE I. ^{59}Co(^{16}O,^{16}O)^{59}Co. Optical model parameters, the real and imaginary Igo constants (C_U and C_W), the strong absorption radii and their corresponding nuclear potentials, and the Coulomb barrier and its radius are given at the bombarding energies of the experiment. Since the barrier height is approximately 38 MeV, the parameters at 36 MeV are poorly determined but are consistent with the values at higher energies.

E_{lab} (MeV)	U (MeV)	W (MeV)	$C_U(10^8)$	$C_W(10^8)$	$D_{1/2}$ (fm)	Re[V_{OM} ($D_{1/2}$)] (MeV)	R_B (fm)	V_B (MeV)	χ^2
36	27.9	37.2	1.7	2.3	...	...	9.10	32.16	0.30
40	71.5	31.1	4.5	1.9	10.23	−0.576 ± 0.057	9.68 ± 0.06	30.43 ± 0.17	0.62
45.5	63.0	24.3	3.9	1.5	10.02	−0.770 ± 0.086	9.60 ± 0.06	30.68 ± 0.20	0.96
49	83.9	15.1	5.2	0.94	10.03	−1.005 ± 0.193	9.78 ± 0.12	30.16 ± 0.32	0.67
52	74.2	23.4	4.6	1.5	9.98	−0.981 ± 0.214	9.70 ± 0.13	30.37 ± 0.38	0.21
56	75.8	21.5	4.6	3.4	9.92	−1.128 ± 0.152	9.71 ± 0.08	30.33 ± 0.23	0.47

$r_R = r_I = 1.22$ fm. $a_R = a_I = 0.5$ fm. $R = r_R(A_T^{1/3} + A_p^{1/3})$. $R_c = 1.22\, A_T^{1/3}$.

ties against variation of the optical model parameters under the constraint of a continuous ambiguity.

Third, the energy dependence of the real and imaginary optical model potentials and associated constants is investigated. Finally, the optical model well depths obtained in this experiment are compared with those for ^{16}O scattering by neighboring nuclides. The solid curves in Fig. 2 represent optical model fits using the computer code *JIB*[10] with Woods-Saxon real and imaginary potentials of the form

$$V_{OM}(r) = -[U(r) + iW(r)] + V_C(r), \tag{1}$$

where

$$U = U_0(1 + e^x)^{-1},$$
$$W = W_0(1 + e^x)^{-1},$$
$$x = \frac{r - R}{a},$$
$$R = r_0(A_t^{1/3} + A_p^{1/3}),$$

and

$$V_C(r) = Z_t Z_p e^2 \begin{cases} \frac{1}{2R_C}\left(3 - \frac{r^2}{R_C^2}\right), & \text{for } r \le R_C \\ \frac{1}{r}, & \text{for } r > R_C. \end{cases} \tag{2}$$

Owing to the relative insensitivity of the results to changes in R_C, its value was set equal to R in all the calculations that follow. To investigate the possible existence of discrete ambiguities, a two parameter search was carried out with a four parameter (U_0, W_0, r_0, a) optical model, holding r_0 and the diffuseness a initially fixed at 1.22 and 0.5 fm, respectively. These values were adopted from previous analyses of ^{16}O scattering.[2,4] Separate geometries for the real and imaginary parts of the optical model potential were also tried. Since no significant improvement was obtained, the same geometry was adopted for both the real and imaginary potentials. Searches were made on U_0 and W_0 for minimum χ^2, defined as

$$\chi_{total}^2 = \sum_{i=1}^{n}\left(\frac{\sigma_{exp} - \sigma_{calc}}{\Delta\sigma_{exp}}\right)_i^2,$$
$$\chi^2 = \chi_{total}^2/(n - p),$$

where χ^2 is the value per point corrected for the number of degrees of freedom since n=(no. of data points) and p=(no. of adjustable parameters). With the geometry fixed, only one minimum in the map of $\chi^2(U, W)$ was found. There is no evidence for discrete ambiguities as illustrated in Fig. 3 for $E_{lab} = 56$ MeV.

TABLE II. Double-folded models' parameters.

E_{lab} (MeV)	α [a]	β [a]	χ^2 [a]	α [b]	W_0 [b] (MeV)	χ^2 [b]
36	0.464	0.597	0.30	0.277	37.12	0.30
40	0.804	0.456	0.69	0.899	31.19	0.62
45.5	0.672	0.661	1.44	0.811	27.81	0.96
49	0.898	0.394	0.69	1.007	25.30	0.62
52	0.803	0.525	0.48	0.919	30.66	0.26
56	0.805	0.570	0.52	0.933	30.88	0.43

[a] Double-folded real and double-folded imaginary.
[b] Double-folded real and Woods-Saxon imaginary.

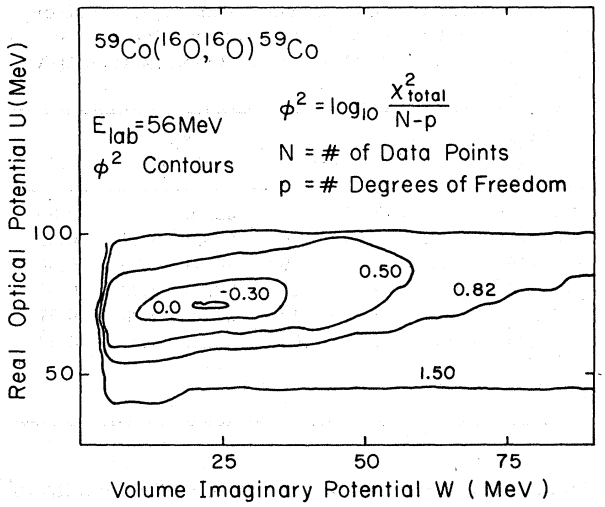

FIG. 3. Contours of constant $\phi^2 = \log_{10}[\chi^2/(n-p)]$ in the U-W plane for $E_{lab} = 56$ MeV.

As expected, continuous ambiguities are evident in the results of ^{16}O scattering on ^{59}Co. As pointed out by Igo,[15] the scattering of highly absorbed particles depends on the tail of the complex potential, the real part of which is approximated, for $r/R \gg 1$, by

$$\mathrm{Re}[V_{\mathrm{OM}}(r)] \simeq -U_0 e^{(R/a)} e^{-(r/a)} + V_C(r) . \tag{3}$$

Equivalent scattering is calculated for any set (a, R, U_0), such that $U_0 e^{R/a} = C_u$ is a constant. This is demonstrated by the nearly constant value of χ^2 in Fig. 4 for $r_0 < 1.35$ fm. A similar expression can be constructed relating W_0, r_0, and a such that $W_0 e^{R/a} = C_W$ is a constant. For small values of r_0, the ambiguity expression for W_0 is satisfied, as seen in Fig. 4, but the points rise above the calculated line for $r_0 > 1.25$ fm. Values of the Igo constants for each energy are given in Table I.

The connection between the Igo ambiguity and the uniqueness of the Coulomb barrier V_B and its radius R_B has been discussed by West *et al.*[2] for ^{16}O elastic scattering by even mass nickel isotopes. By definition, the barrier height V_B is given by

$$V_B = \mathrm{Re}[V_{\mathrm{OM}}(R_B)] = -\frac{U_0}{1+\exp[(R_B - R)/a]} + V_C(R_B) . \tag{4}$$

When $(R_B - R) \gg a$, V_B is approximated by

$$V_B \simeq -U_0 \exp\left(\frac{R - R_B}{a}\right) + V_C(R_B) \simeq -C_u \exp(-R_B/a) + V_C(R_B) , \tag{5}$$

which relates V_B, R_B, and the Igo ambiguity constant.

To the extent that V_B and R_B are determined by the experimental cross sections, Eq. (5) suggests

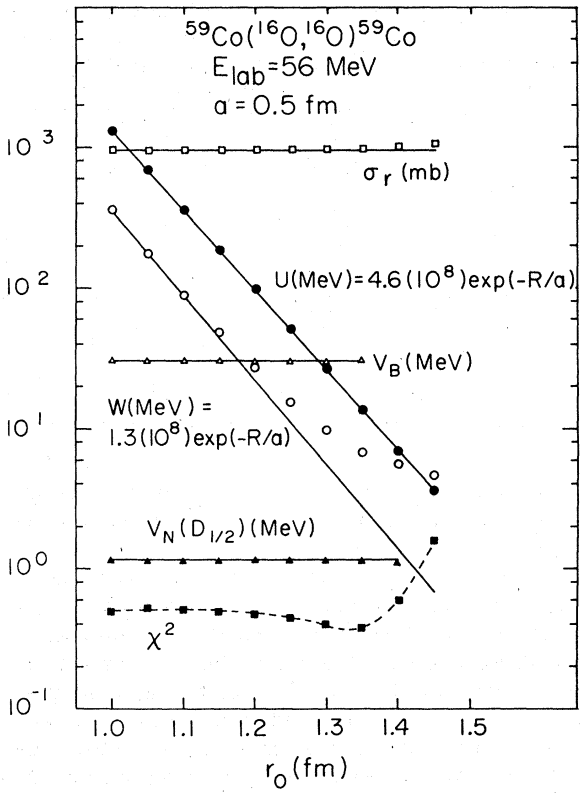

FIG. 4. The values of the real and imaginary potential well depths for which χ^2 is a minimum at 56 MeV for different values of r_0. The corresponding values of the Coulomb barrier V_B, the nuclear potential at the strong absorption radius $V_N(D_{1/2})$ (see text), and total reaction cross sections are shown. The diffuseness value is $a = 0.50$ fm.

that any values of U_0, R, and a which hold

$$C_B = U_0 \exp\left(\frac{R - R_B}{a}\right) \tag{6}$$

constant will provide a reasonable fit to the data. Figure 5 shows the loci of best fit $(U_0, 1/a)$ and $(W_0, 1/a)$ for $r_0 = 1.22$ fm. Again, the ambiguity expression for the real potential holds over a longer range of $1/a$ than does that for W_0.

As seen in Figs. 4 and 5, the barrier height V_B is rather accurately determined by the data. The value is about 20% lower than that obtained from the definition of the "ordinary" Coulomb barrier $Z_t Z_p e^2/R$, consistent with the results obtained by Obst *et al.*[1]

The quantity which is most precisely determined by elastic scattering at one bombarding energy is the real nuclear potential at the strong absorption radius, $\mathrm{Re}[V_{\mathrm{OM}}(D_{1/2})]$.[4,8,9] This illustrated for 56-MeV data by the curve labeled $V_N(D_{1/2})$ in Figs. 4 and 5 which is even more stable than V_B.

The strong absorption radius $D_{1/2}$ is computed

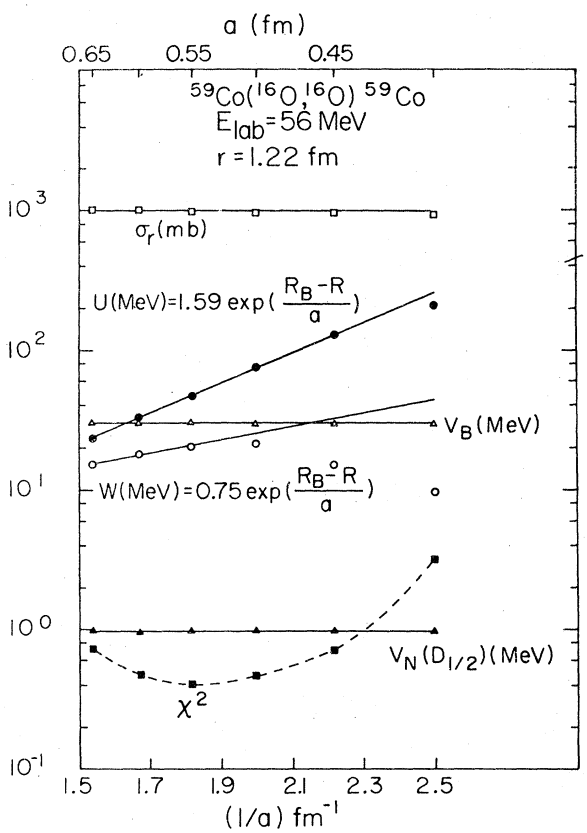

FIG. 5. The values of the real and imaginary potential well depths for which χ^2 is the minimum as a function of the reciprocal of the diffuseness ($1/a$) at E_{lab} = 56 MeV with r_0=1.22 fm. The corresponding values of the Coulomb barrier V_B, the nuclear potential at the strong absorption radius $V_N(D_{1/2})$ (see text), and total reaction cross sections are shown.

from the formula for the distance of closest approach for Coulomb trajectories:

$$D_{1/2}=\frac{\eta}{k}\{1+[1+(L_{1/2}/\eta)^2]^{1/2}\}, \tag{7}$$

where η is the usual Sommerfeld parameter $Z_t Z_p e^2/\hbar v$, k is the wave number, and $L_{1/2}$ is the partial wave for which the transmission coefficient is $\frac{1}{2}$. These values have been computed from the four parameter optical model output. They are listed in Table I for the bombarding energies of this experiment along with values for the optical model parameters, R_B, V_B, and the nuclear potential at the strong absorption radius $\mathrm{Re}[V_{OM}(D_{1/2})]$. Values for the total reaction cross section are tabulated separately and will be discussed in Sec. IV.

The real optical model potential at $D_{1/2}$ can be expressed by

$$\mathrm{Re}[V_{OM}(D_{1/2})]=-\frac{U_0}{1+\exp(D_{1/2}-R)/[a]}. \tag{8}$$

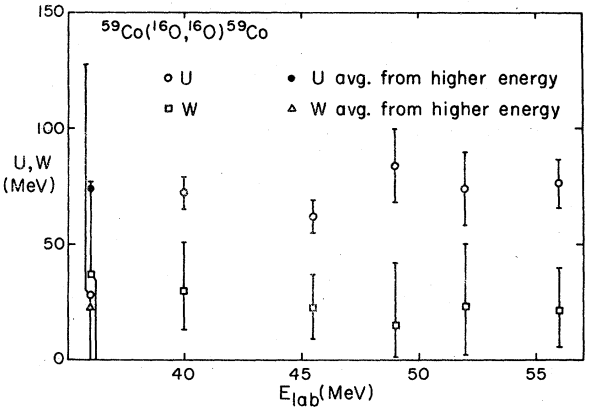

FIG. 6. The value of the real and imaginary potential well depths U and W, respectively, as functions of the bombarding energy for ^{16}O scattering from ^{59}Co.

When $(D_{1/2}-R)\gg a$, Eq. (8) is approximated by

$$\mathrm{Re}[V_{OM}(D_{1/2})]\simeq -U_0\exp\left(\frac{R-D_{1/2}}{a}\right), \tag{9}$$

the magnitude of which is labeled by $V_N(D_{1/2})$ in Figs. 4 and 5. Because the real part of the potential at the strong absorption radius is precisely determined by elastic scattering data at one energy, i.e., $V_N(D_{1/2})$ = constant in Figs. 4 and 5, Eq. (9) is a continuous ambiguity relation which is very well satisfied.

The U_0 and W_0 values which best describe the angular distributions at each energy are plotted in Fig. 6. The uncertainty assigned to U_0 was determined from the criterion,[16]

$$\chi^2(U_0+\Delta U, W_0)=\chi_{\min}^2(U_0,W_0)+1,$$

and a similar criterion was used for the uncertainty in W_0. No systematic energy dependence for U_0 and W_0 is suggested by Fig. 6 and horizontal lines can be drawn through the uncertainty bars for both U_0 and W_0. The large uncertainty bars assigned to the U_0 and W_0 values at 36 MeV are expected since the bombarding energy is significantly below the barrier (≃38 MeV lab) and consequently the optical model parameters are poorly determined. As seen in Fig. 6, average values of U_0 and W_0 determined from the higher energy data ($E_{lab}\geq 40$ MeV) fall within the uncertainty bars of the values determined at 36 MeV.

When compared with neighboring Ni isotopes,[2] the ^{59}Co nucleus appears to be more absorbing at all energies studied here. A comparison is shown in Fig. 7 for ^{16}O on ^{58,60}Ni and ^{59}Co at $E_{lab}=40$. Average values of U_0 and W_0 for the scattering of ^{16}O by a number of target nuclei are plotted against target A in Fig. 8. These average values of U_0 and W_0 have been obtained with the same geometrical parameters for all target nuclei. The ^{16}O+^{59}Co sys-

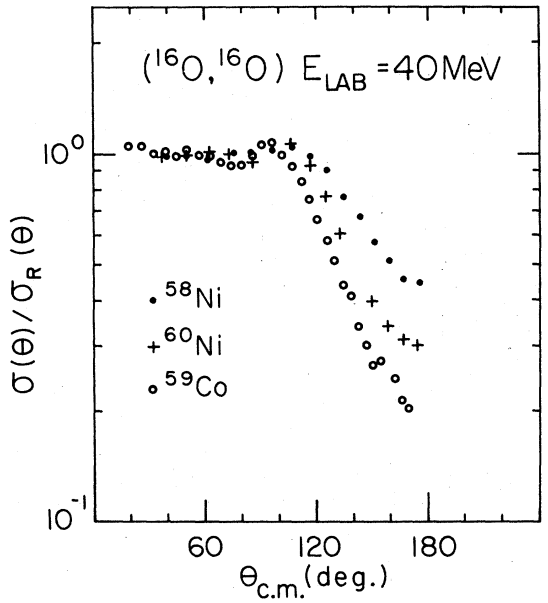

FIG. 7. Experimental angular distributions for the elastic scattering of ^{16}O from ^{58}Ni, ^{59}Co, and ^{60}Ni at E_{lab}=40 MeV which illustrates the more absorptive nature of ^{59}Co(^{16}O, ^{16}O)^{59}Co system.

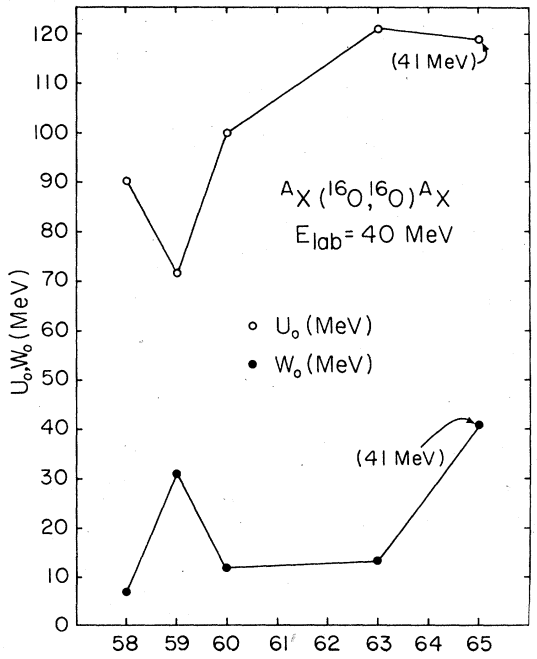

FIG. 8. The values of the real and imaginary potential well depths as function of the atomic mass A, for isotopes with $A \sim 60$. The same r_0 and a values are used throughout and the U_0 and W_0 values are averages over comparable energy ranges.

tem has a larger imaginary well depth W and a smaller real optical potential than do the Ni isotopes or ^{63}Cu for 40-MeV bombarding energy.

B. Double-folded real potential calculations

The justification for the common use of the optical model in the analyses of heavy ion scattering is more pragmatic than physical. Since the interaction originates in the nucleon-nucleon potential operating between many nucleon pairs in both the projectile and target, a more satisfactory heavy ion interaction model is one which explicitly accounts for the interaction of a nucleon in one nucleus with the nucleons in the other. Such a model is the G-matrix double-folding model mentioned earlier.[4,8,9] In this model the real part of the optical potential is obtained by the double-folding of a G-matrix interaction[17] with realistic density distributions describing the projectile and target ground states. The model is expected to give a reasonable estimate of the real nuclear potential only in the region $r \gtrsim D_{1/2}$ which is adequate for elastic scattering. For further details the reader is referred to Refs. 4, 8, and 9.

In the present calculations oscillator distributions with parameters obtained from electron scattering[18] were used to describe the ^{16}O projectile. The Woods-Saxon density parameters given by the droplet model of Myers[19] were used to describe the ^{59}Co target. The calculations were made with the computer code *JIB* modified by Stanley and Golin.[10]

Two form factors were used for the imaginary part of the potential, the double-folded form factor and the Woods-Saxon expression, i.e.,

$$U_{opt}(r) = \begin{cases} \alpha(1+i\beta)U_{folded}(r), & (10) \\ \alpha U_{folded} + iW_0 f(r), & (11) \end{cases}$$

where

$$f(r) = (1+\exp\{[r - r_0(A_p^{1/3} + A_t^{1/3})]/a\})^{-1}, \quad (12)$$

$$U_{folded}(r) = \int d\vec{r}_p d\vec{r}_t \rho_p(\vec{r}_p)\rho_t(\vec{r}_t) g(s),$$

$$s \equiv (|\vec{r} + \vec{r}_p - \vec{r}_t|). \quad (13)$$

In Eq. (13) the ρ's are the densities and g is the G-matrix interaction. When the form given by Eq. (10) was used α and β were varied to minimize χ^2. When the form given by Eq. (11) was used r_0 and a were fixed at 1.22 and 0.50 fm, respectively, and α and W_0 were varied to minimize χ^2.

In the analysis in which both the real and imaginary potentials had the double-folded forms, Eq. (10), the normalization factors ranged from 0.7 to 0.9 for α and 0.4 to 0.6 for β in the bombarding energy range 40–56 MeV. With a double-folded real potential and a Woods-Saxon imaginary potential [Eq. (11)] the analysis yielded 0.8 to 1.0 for α and 25 to 31 MeV for W_0 again neglecting the below barrier point at E_{lab}=36 MeV. Numerical results are given in Table II and plotted in Fig. 9. The fits to the data are very good and comparable

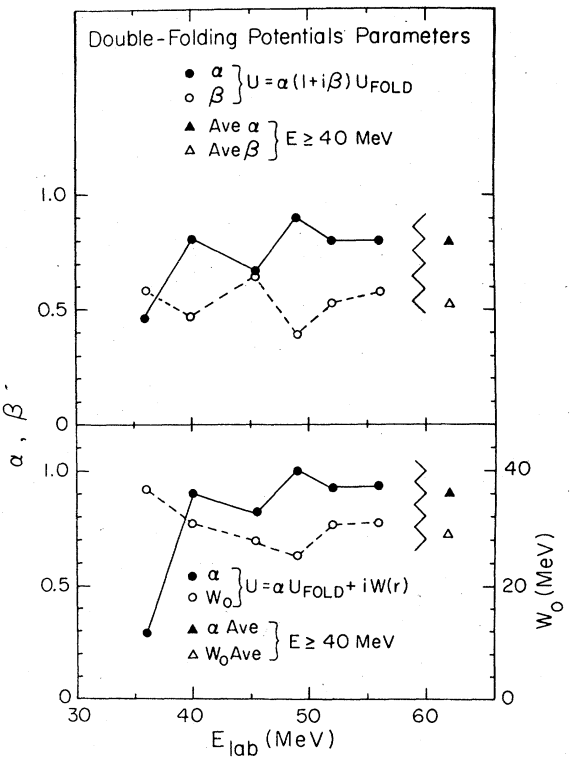

FIG. 9. The values of the normalization factors α and β for the double-folding real and imaginary potentials, and the values of the normalization factor α for the double-folding real, and the Woods-Saxon imaginary potentials W_0 as functions of the bombarding energy.

with those obtained with the optical model (see Fig. 2, Tables I and II). A particularly satisfying result of the double-folding analysis is the near unity range of values found for α, the strength normalization factor for the real potential.

IV. TOTAL REACTION CROSS SECTIONS

Potential models for heavy ion scattering such as the optical model or doubel-folded models incorporate specifically nuclear mechanisms for depleting the elastic channel flux and yield a value of the total reaction cross section. Without modification, these models do not incorporate the Coulomb excitation which can represent a significant contribution to the total reaction cross section as shown by Thorn *et al.*[20] Recently, a theory of dynamic Coulomb excitation has been discussed by Love *et al.*[21]

The typical total reaction cross section for heavy ions rises monotonically with increasing bombarding energy and asymptotically approaches a geometric limit. An exception to the monotonic rise in the total reaction cross section is expected for light-heavy ions for which absorption is relatively low as pointed out by Philpott.[22] Structure in the excitation curve occrus when the energy interval between successive partial-wave absorption is sufficiently large that the contribution of the partial wave just absorbed markedly decreases (proportional to $1/E$) before the rapid rise of the next partial-wave contribution. Where the total reaction cross section is dominated by one mechanism, for example fusion, structure due to successive partial-wave absorption will be reflected in the excitation curve for the fusion reaction as suggested elsewhere.[7] Sperr *et al.*[23] have reported structure in the fusion cross section for light-heavy ions, in particular reacting pairs for which the absorption is small.

In this section the total reaction cross sections for ^{16}O on ^{59}Co are extracted using scattering potential models, the Fresnel quarter-point method,[6] a "half partial-wave" method, and a model independent sum-of-differences (SOD) method.[3,5]

A. Total reaction cross section from optical model and double-folded potential models

The total reaction cross sections for ^{16}O on ^{59}Co obtained by optical model analysis are given in Table III and shown in Fig. 10. As expected from the equivalence of the fits to the data, the total reaction cross section values determined from the double-folded models is in good agreement with those obtained from the optical model. The values are insensitive to the changes in the optical model geometry provided that continuous ambiguity relations are satisfied as can be seen from Fig. 11 for $E_{lab}=56$ MeV. Except for the SOD values, the determinations in Fig. 10 do not specifically include the contribution from Coulomb excitation which suggests that the SOD values should be consistently higher as observed. An account of this difference by possible Coulomb excitation is taken up in a later subsection.

B. Fresnel model and the quarter-point method

Frahn[6] showed that the ratio of the elastic differential cross section $\sigma_{el}^{(\varphi)}$ to the Rutherford differential cross section $\sigma_r(\theta)$ is given by

$$\sigma_{el}(\theta)/\sigma_R(\theta)=\tfrac{1}{2}\{[\tfrac{1}{2}-S(\alpha)]^2+[\tfrac{1}{2}-C(\alpha)]^2\}, \qquad (14)$$

where $S(\alpha)$ and $C(\alpha)$ are the Fresnel sine and cosine integrals of argument

$$\alpha=\left(\frac{\eta}{2\pi}\right)\csc\left(\frac{\theta_{1/4}}{2}\right)\sin[\tfrac{1}{2}(\theta-\theta_{1/4})]. \qquad (15)$$

η is the usual Sommerfeld parameter and $\theta_{1/4}$ is the center-of-mass angle determined from the experimental angular distribution for which the ratio to Rutherford is $\frac{1}{4}$. In this analysis, the total

TABLE III. Total reaction cross section.

E_{lab} (MeV)	OM (mb)	$\frac{1}{2}$-Partial wave (mb)	$\frac{1}{4}$-pt. (mb)	SOD (mb)	D-F[a] (mb)	D-F[b] (mb)	Coulomb excitation cross section (mb)
36	22	...	...	42	22	23	39
40	176	155	...	201	183	173	62
45.5	482	479	423	520	515	480	100
49	677	691	638	711	699	679	129
52	813	819	775	899	838	814	153
56	963	969	938	1116	1002	968	188

[a]Double-folded real and double-folded imaginary.
[b]Double-folded real and Woods-Saxon imaginary.

reaction cross section can be obtained from

$$\sigma_r = \pi\lambda^2(l_{max}+1)^2 , \quad (16)$$

where l_{max} is the maximum angular momentum for which particles take part in the reaction:

$$l_{max}+\tfrac{1}{2} = \eta \cot\frac{\theta_{1/4}}{2} . \quad (17)$$

All the values for the total reaction cross sections that can be evaluated by this method are listed in Table III. The agreement is good, and is in most cases, well within 10%. At energies near the Coulomb barrier, the calculation is not possible since the ratio to Rutherford is everywhere larger than $\frac{1}{4}$.

C. "Half partial-wave" method

This method is an extension of the Fresnel quarter-point method to a lower energy, but still above the barrier. The total reaction cross section, Eq. (16), is used with l_{max} replaced by $L_{1/2}$ defined as the angular momentum of the first partial wave for which the transmission drops to $\frac{1}{2}$. With these definitions, values for the total reaction cross sections were calculated and are presented in Table III. As expected since the transmission coefficients are evaluated with the optical model, these values are in better agreement with the optical model values than those obtained from the quarter-point method. The advantage to this method over the quarter-point method lies in the fact that there are energies near but above the Coulomb barrier such that there exists a partial wave for which the transmission or reflection is $\frac{1}{2}$, but $\sigma/\sigma_R > \frac{1}{4}$.

D. Sum-of-differences method

In the previous subsections the total reaction cross sections were obtained using various mod-

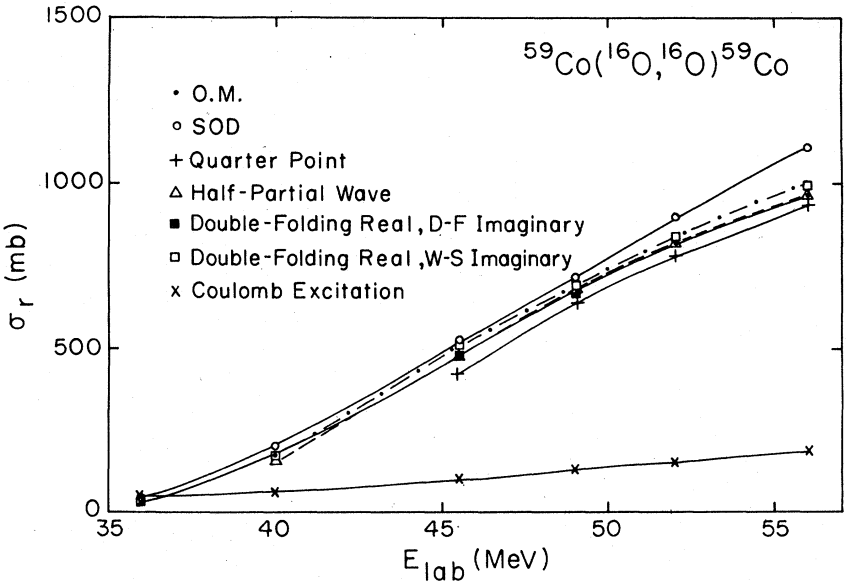

FIG. 10. The values of the total reaction cross sections, evaluated by the various methods (see text) and the estimated Coulomb excitation cross section, as a function of the bombarding energy.

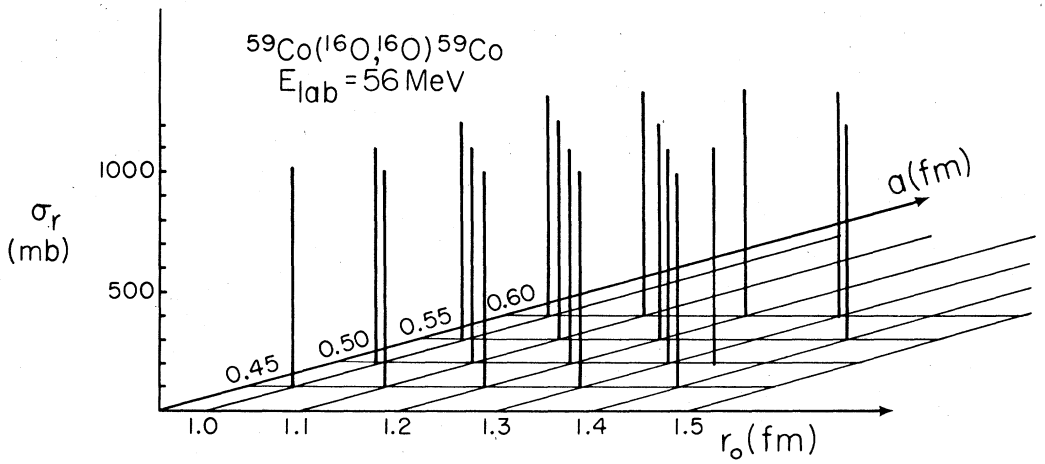

FIG. 11. The values of the total reaction cross section for $E_{lab}=56$ MeV as a function of r_0 and diffuseness a. Other parameters are determined by continuous ambiguity relations.

els for heavy ion scattering. The scattering potential models explicitly incorporate and the quarter-point and half partial-wave methods implicitly take into account the short range nuclear forces and the long range Coulomb forces involved in heavy ion collisions. Moreover, the quarter-point and the half partial-wave methods require sufficient absorption to satisfy the respective conditions for selecting a characteristic l value.

The short range of the nuclear force, the long range of the Coulomb force, and the high reaction probability in heavy ion collisions are directly exploited in the sum-of-differences method (SOD) to determine the total reaction cross section from heavy ion elastic scattering angular distributions.[3,5] The condition for the validity of the semiclassical SOD method is the existence of a measurable segment of the angular distribution which is Rutherford within experimental error, i.e., there exists an angle θ_1, such that the measured ratio to Rutherford is unity for $\theta \leq \theta_1$. All of the angular distributions in Fig. 2 show this "typical" feature. Associated with θ_1 is an impact parameter b_1 such that the area πb_1^2 contains all of the reaction cross sections plus the integrated elastic scattering cross section from θ_1 to 180°,

$$\pi b_1^2 = \sigma_r + \int_0^{2\pi}\int_{\theta_1}^{\pi} \sigma_{el}(\theta) d\Omega \,, \tag{18}$$

since

$$\pi b_1^2 = \int_0^{2\pi}\int_{\theta_1}^{\pi} \sigma_R(\theta) d\Omega \,, \tag{19}$$

the total reaction cross section, is obtained from the measured elastic scattering differential cross section $\sigma_{el}(\theta)$,

$$\sigma_r = \int_0^{2\pi}\int_{\theta_1}^{\pi} [\sigma_r(\theta) - \sigma_{el}(\theta)] d\Omega \,, \tag{20}$$

without recourse to other models.

Holdeman and Thaler,[11] and more recently Schwarzschild *et al.*[24], applied the optical theorem to charged particle scattering and obtained an expression for the total reaction cross section

$$\sigma_r = \int_0^{2\pi}\int_{\theta_1}^{\pi} [\sigma_R(\theta) - \sigma_{el}(\theta)] d\Omega + \Delta \,, \tag{21}$$

which differs from the result in Eq. (20) by the additional term Δ. In the SOD method, $\Delta = 0$. Holdeman and Thaler derived an approximate expression for Δ which can be written as

$$\Delta = \frac{4\pi}{k} \mathrm{Im}\left\{ f'(0°) \exp\left[2i\left(\eta \ln \sin\frac{\theta_1}{2} - \sigma_0 \right) \right] \right\} - 4\pi |f'(0°)|^2 \sin^2\frac{\theta_1}{2} \,, \tag{22}$$

where $f'(0°)$ is the residual nuclear amplitude at 0° given by

$$f'(0°) = \frac{1}{2ik} \sum_{l=0}^{\infty} (2l+1) \exp(2i\sigma_l) \exp(2i\delta_l - 1) \,. \tag{23}$$

η is the Sommerfeld parameter, σ_l are the Coulomb phase shifts, and δ_l are the nuclear phase shifts. The equation for Δ is valid for small θ_1 since the residual nuclear amplitude $f'(0°)$ is evaluated at 0°. This approximation was used in the estimate of Δ by Wojciechowski *et al.*[5]

To formulate the Δ function accurately for larger θ_1, the exact expression must be used,

$$\Delta = -\lim_{n\to\infty} \left[2\pi \int_{\epsilon_n}^{\theta_1} |f'(\theta)|^2 \sin\theta \, d\theta + 4\pi \,\mathrm{Re} \int_{\epsilon_n}^{\theta_1} f_C^*(\theta) f'(\theta) \sin\theta \, d\theta \right] + \frac{4\pi}{R} \mathrm{Im} f'(0°) \,, \tag{24}$$

where $\epsilon_n = 2\exp\left(\frac{\sigma_0 - n\pi}{\eta}\right)$

with

$$f'(\theta) = \frac{e^{2i\sigma_0}}{2ik}\sum_{l=0}^{L_{max}}(2l+1)e^{2i\omega_l}(S_l - 1)P_l(\cos\theta), \quad (25)$$

$$\omega_l = \sigma_l - \sigma_0 = \sum_{l'=1}^{l}\tan^{-1}\left(\frac{\eta}{l'}\right), \quad (26)$$

and

$$f_C(\theta) = \frac{\eta}{2k\sin^2(\theta/2)}e^{i[2\sigma_0 + \pi - \eta\ln\sin^2(\theta/2)]}. \quad (27)$$

Computational difficulties arise in the evaluation of the integrals because of the large amplitudes and rapid oscillations of the integrands as θ becomes small.

Two plots of Δ as a function of starting angle θ_1 are shown in Fig. 12 for the analysis at 56 MeV. Curve a is calculated using the Holdeman and Thaler[11] approximation which is accurate for very small θ_1. As θ_1 approaches zero the amplitude of Δ is constant and small compared with the value of the total reaction cross section, ~1,000 mb. The inadequacy of the Holdeman and Thaler approximation as θ_1 increased is illustrated by a comparison with curve b which was calculated with the exact expression for Δ. It is clear that the Holdeman and Thaler approximation (curve a) has failed for an angle as large as 6°. An attempt to smoothly join the two curves at an angle sufficiently small that the Holdeman and Thaler expression was still valid was frustrated by computational difficulties in extending the exact calculation to smaller angles. Using a 32-point Gaussian quadrature integration method, the envelope of the Δ amplitude blows up as the starting angle for curve b is reduced below 5°. Curve b was truncated at that point since the envelope of Δ diverges rather than converges to the envelope of the Holdeman and Thaler curve a as it must for small θ_1.

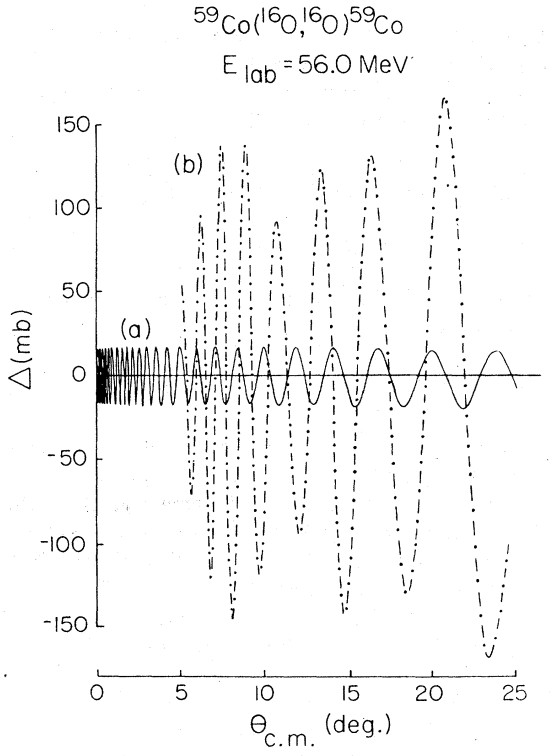

FIG. 12. The quantum mechanical correction Δ as a function of starting angle, (a) using the Holdeman and Thaler approximation, and (b) an exact evaluation of the integral by use of a 32-point Gaussian quadrature integration method.

Using the Holdeman and Thaler approximation of Eq. (22) the amplitudes of Δ are less than 2% of the total reaction cross section at higher energies and decrease with decreasing energy as shown in Fig. 13. Where the exact expression can be reliably calculated at larger angles for 56 MeV, the Δ amplitudes are approximately 10% of the total reaction cross section and increase with angle. As in the case of the Holdeman and Thaler approximation, Δ amplitudes calculated with the exact expression decrease with decreasing energy.

The calculation of Δ requires knowledge of the phase shifts obtained by some means, the optical model in this case. Estimates of Δ do provide a theoretical measure of the error in SOD, but one which is subject to the errors in the phase shifts used in the calculation.

As seen in Fig. 12, Δ oscillates rapidly as a function of the starting angle θ_1 so that for a number of randomly chosed starting angles, the average value of Δ is approximately zero. In an ap-

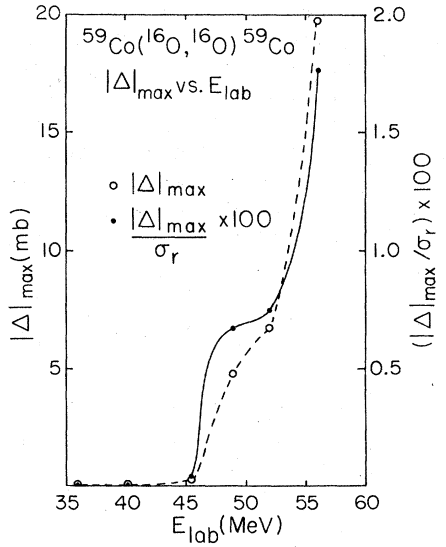

FIG. 13. The amplitude of Δ determined by the Holdeman and Thaler approximation as a function of the bombarding energy.

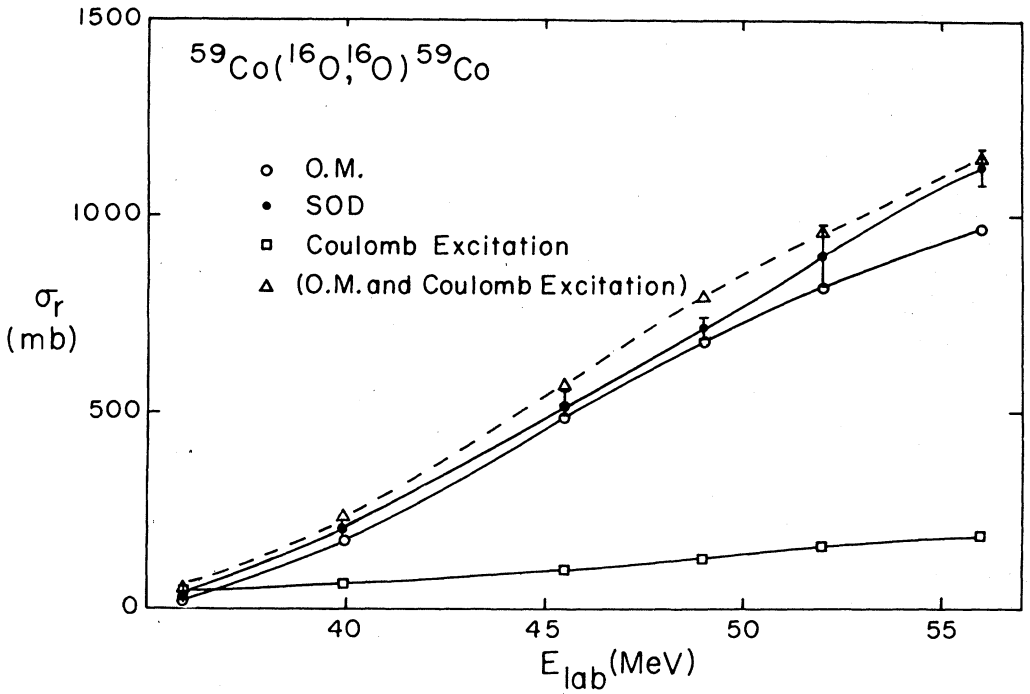

FIG. 14. The values of the total reaction cross section obtained by the optical model (OM) and SOD, the estimaed Coulomb excitation cross section and the sum of OM total reaction cross section and the estimated Coulomb excitation (see text) as a function of bombarding energy.

plication of the SOD method to data, a number of forward angle points are used to fix the Rutherford scattering segment of the angular distribution, and these points are randomly chosen with respect to oscillations of Δ. There are minute differences in σ_r determined by SOD depending on which experimental point is chosen as the initial angle, but the major contribution to the experimental error in the SOD method is the error in the normalization of the Rutherford scattering segment. This depends, of course, on the precision of forward angle data. For example, an assumed $\frac{1}{2}\%$ error in Rutherford normalization produced the error bars in the SOD values in Fig. 14. This error is equally applicable to the optical model values of the total reaction cross section.

As mentioned earlier the SOD technique produces a total reaction cross section due to all reactions which deplete the elastic flux. In particular the yield of Coulomb excitation is included in SOD estimates consistent with the fact that the SOD values are somewhat higher than those obtained using an optical model alone. Of course part of the Coulomb excitation yield is accounted for by the tail of the imaginary part of the optical model potential. Thus the SOD total reaction cross section is not expected to be simply a sum of the optical model total reaction cross section plus the Coulomb excitation contribution. Nonetheless, this simple sum relation was investigated by estimating the Coulomb excitation cross section of the lowest six closely spaced excited states from results of previous experiments[25,26] since the inelastic yield was not resolvable in this experiment. Coulomb excitation cross section estimates are presented in Table III. A plot of the sum of optical model total reaction cross section plus Coulomb excitation contribution is given in Fig. 14 and compared with the total reaction cross section obtained by the SOD method. The sum of the optical model and the Coulomb excitation values is somewhat larger than the SOD values but generally within the error bars assigned to SOD only.

ACKNOWLEDGMENTS

The authors wish to thank F. Petrovich and D. P. Stanley for making available the double-folding code and for their valuable suggestions during the data analyses. Thanks are extended to J. Purcell for the helpful discussions concerning the application of the optical theorem to heavy ion scattering. The assistance of L. Fry during the data acquisition and the contribution of R. V. LeClair to code development are gratefully acknowledged. The authors are indebted to V. Hnizdo of the University of the Witwatersrand, Johannesburg for a careful reading of the manuscript and the correction of an error in the calculation. This work was supported in part by the National Science Foundation.

*Present address: Xerox Corporation, Webster, New York 14580.
[1]A. W. Obst, D. L. McShan, and R. H. Davis, Phys. Rev. C 6, 1814 (1972); A. W. Obst, D. L. McShan, M. B. Greenfield, R. Holub, and R. H. Davis, *ibid.* 8, 1379 (1973).
[2]Leon West, Jr., K. W. Kemper, and N. R. Fletcher, Phys. Rev. C 11, 859 (1975).
[3]H. Wojciechowski, D. E. Gustafson, L. R. Medsker, and R. H. Davis, Phys. Rev. Lett. 63B, 413 (1976); Proceedings of the Symposium on Macroscopic Features of Heavy Ion Collisions, 1976, Argonne National Laboratory Report No. ANL/PHY-76-2 (unpublished).
[4]H. Wojciechowski, N. B. J. Tannous, R. H. Davis, D. Stanley, M. Golin, and F. Petrovich, Phys. Rev. C 17, 2126 (1978).
[5]H. Wojciechowski, L. R. Medsker, and R. H. Davis, Phys. Rev. C 16, 1767 (1977).
[6]W. E. Frahn, Ann. Phys. (N.Y.) 72, 524 (1972).
[7]R. H. Davis, International Conference on Resonance in Heavy Ion Reactions, Hvar, Yugoslavia, 1977 (unpublished).
[8]G. R. Satchler, Proceedings of the Symposium on Macroscopic Features of Heavy Ion Collisions, Argonne, 1976, Argonne National Laboratory Report (unpublished), V. 1, p. 32; R. Satchler and W. C. Love, Phys. Rev. Lett. 65B, 415 (1976).
[9]M. Golin, F. Petrovich, and D. Robson, Phys. Lett. 64B, 253 (1976); D. Stanley, M. Golin, and F. Petrovich, submitted to Nucl. Phys.
[10]F. G. Perey, Phys. Rev. 131, 745 (1963); A. W. Obst, Florida State University Technical Report JIB, 1973 (unpublished); D. Stanley and M. Golin, report (unpublished).
[11]J. T. Holdeman and R. M. Thaler, Phys. Rev. Lett. 14, 81 (1965); Phys. Rev. 139, B1186 (1965).
[12]K. R. Chapman, Nucl. Instrum. Methods 124, 229 (1975); IEEE Trans. Nucl. Sci. NS-23, 1109 (1976).
[13]E. J. Feldl, P. B. Weiss, and R. H. Davis, Nucl. Instrum. Methods 28, 309 (1964).
[14]See AIP document No. PAPS PRVCA 18-2190-8 for pages of experimental angular distribution data for $^{59}Co(^{16}O,^{16}O)^{59}Co$ at E_{lab} = 36–56 MeV. Order by PAPS number and journal reference from American Institute of Physics, Physics Auxiliary Publications Service, 335 East 45th Street, New York, New York, 10017. The price is $1.50 for microfiche or $5 for photocopies. Airmail additional. Make checkes payable to the American Institute of Physics. This material also appears in *Current Physics Microfilm*, the monthly microfilm edition of the complete set of journals published by AIP, on frames immediately following this journal article.
[15]G. Igo, Phys. Rev. Lett. 1, 1 (1958); Phys. Rev. 115, 1665 (1959).
[16]P. R. Bevington, *Data Reduction and Error Analysis for the Physical Sciences* (McGraw-Hill, New York, 1969).
[17]G. Bertsch, J. Borysowicz, H. McManus, and W. G. Love, Nucl. Phys. A284, 399 (1977).
[18]C. W. de Jager, H. de Vries, and C. de Vries, At. Data Nucl. Data Tables 14, 479 (1974).
[19]W. D. Myers, Nucl. Phys. A145, 387 (1970).
[20]G. E. Thorn, M. J. LeVine, J. J. Kolata, C. Flaum, P. D. Bond, and J. D. Seus, Phys. Rev. Lett. 38, 384 (1977).
[21]W. G. Love, T. Terasawa, and G. R. Satchler, Phys. Rev. Lett. 39, 6 (1977).
[22]R. J. Philpott, Phys. Rev. C 12, 1540 (1975).
[23]P. Sperr, T. H. Braid, Y. Eisen, D. G. Kovar, F. N. Prosser, Jr., J. P. Schiffer, S. L. Tabor, and S. Vigdor, Phys. Rev. Lett. 37, 321 (1976).
[24]A. Z. Schwarzschild, E. H. Auerbach, R. C. Fuller, and S. Kahana, report, Brookhaven National Laboratory, Upton, N. Y., 1973 (unpublished).
[25]R. Nordhagen, B. Elbek, and B. Herskind, Nucl. Phys. A104, 353 (1967).
[26]H. J. Kim Nucl. Data Sheets 17, 505 (1976).